ACS Biomaterials SCIENCE & ENGINEERING

pubs.acs.org/journal/abseba Article

Brain-on-a-Chip Device for Modeling Multiregional Networks

Kenneth Ndyabawe, Michael Cipriano, Wujun Zhao, Mark Haidekker, Kun Yao, Leidong Mao, and William S. Kisaalita*

Cite This: *ACS Biomater. Sci. Eng.* 2021, 7, 350–359 Read Online

ACCESS | Metrics & More | Article Recommendations

ABSTRACT: Animal models are frequently used in drug discovery because they represent a mammalian in vivo model system, they are the closest approximation to the human brain, and experimentation in humans is not ethical. Working with postmortem human brain samples is challenging and developing human in vitro systems, which mimic the in vivo human brain, has been challenging. However, the use of animal models in drug discovery for human neurological diseases is currently under scrutiny because data from animal models has come with variations due to genetic differences. Evidence from the literature suggests that techniques to reconstruct multiple neurotransmission projections, which characterize neurological disease circuits in humans, in vitro, have not been demonstrated. This paper presents a multicompartment microdevice for patterning neurospheres and specification of neural stem cell fate toward networks of multiple neuronal phenotypes. We validated our design by specification of human neural stem cells to dopaminergic and GABAergic neurons in different compartments of the device, simultaneously. The neurospheres formed unrestricted robust neuronal circuits between arrays of neurospheres in all compartments of the device. Such a device design may provide a basis for formation of multineurotransmission circuits to model functional connectivity between specific human brain regions, in vitro, using human-derived neural stem cells. This work finds relevance in neurological disease modeling and drug screening using human cell-based assays and may provide the impetus for shifting from animal-based models.

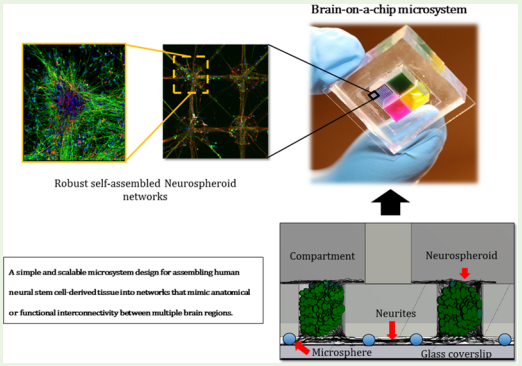

KEYWORDS: *brain-on-a-chip, neural stem cells, microfabrication, neurological disease models, 3D neuronal tissue, drug discovery*

1. INTRODUCTION

The human brain's total structural and functional organization is made up of distinct neuroanatomical hierarchies, which possess distinct cellular organization but work in concert to execute specific functionality. Therefore, neural circuits for neurological diseases and other neurophysiological phenomena, such as addiction, emotion (anxiety/depression), and motor control, are made up of networks, which constitute multiple brain regions. For example, deficits in schizophrenia are thought to originate from dysregulation of dopaminergic, glutamatergic, or GABAergic transmission in the mesocortical and mesolimbic pathways, which are made of prefrontal cortex (PFC), ventral tegmental area (VTA), striatum, substantia nigra, and hippocampal regions.[1,2] Another example of multiregion information exchange is in depression and anxiety circuitry where glutamatergic and GABAergic neurons from different brain regions, such as the lateral habenula, PFC, hypothalamus, substantia nigra, amygdala, and preoptic area, modulate serotonergic transmission in the dorsal raphe nucleus.[3] Because animal brains are thought to duplicate the functional and anatomical connectivity of human brain networks, research to understand human brain physiology commonly utilizes animal models or animal ex vivo brain tissues. However, use of animal models is under scrutiny due to species differences in inflammation response, neural plasticity,[4,5] etc. Such differences are suspected to result in knowledge gaps, which may translate to a high failure rate of drugs. It is estimated that only one-third of drug research conducted in animals can be translated to human clinical trials,[6] and only 8% of the drugs that enter clinical trials pass phase I.[7]

Human 3D cell-based models have been demonstrated to have the potential to produce microtissues that mimic certain aspects of neurophysiology, such as cortical laminar organization and formation of excitatory synapses in cortical neurons,[8,9] and phenotypic specific neurotoxicity.[10] However, cellular models for disease, which utilize neuronal phenotypes representative of a single brain region, are not likely to

Received: June 15, 2020
Accepted: November 5, 2020
Published: December 15, 2020

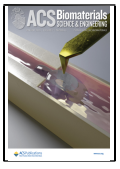

recapitulate in vivo behavior because local electrophysiological properties of neuronal populations, such as spike frequency and interspike interval, are shaped by feedback loops that occur via communication with other interacting regions.[11] Therefore, such models may be of limited application if they do not recapitulate functional connectivity hierarchies associated with neurophysiological phenomena.

A means to model inter-regional connectivity linked to brain functionality using human cell-based models is likely to improve the relevance of in vitro models in neuropharmacology and other neurological disease studies.[12] In this study, we will demonstrate a multicompartment device design to facilitate formation of 3D neuronal networks between two different neuronal phenotype circuits. Key objectives of the design were first, to develop a compact design to facilitate scalability and integration into existing multiwell platforms for high density drug screening; second, to minimize diffusion of chemical agents between compartments of the device. We co-differentiated human neural stem cells to dopamine and γ-aminobutyric acid (GABA) neurons in different compartments of the device, which connected to form dopamine−GABA circuitry. Such circuitry is a potential model for VTA−nucleus accumbens (NAc) network and a basis for modeling functional inter-regional connectivity in a human brain, in vitro. Interactions between dopaminergic neurons in the VTA and GABAegic neuron in the NAc are the core of the mesolimbic pathway,[13,14] which is mainly associated with reward/aversion-related cognition and addiction.[15] Also, information exchange between the VTA and NAc mediates deficits such as cognitive[16] and positive symptoms in schizophrenia[17,18] and its treatment side effects.[19] Such a device may find application in neurological studies that model drug-induced feedback response and side effects between connected brain regions.

2. MATERIALS AND METHODS

2.1. Device Design and Fabrication. The device was made of a four-compartment cell culture medium reservoir (divider box) and a thin PDMS membrane with through-holes for the culture of neuropsheres. To fabricate the PDMS substrate for cell culture, a small amount of polydimethylsiloxane (PDMS) prepolymer was poured onto the SU8 mold on a silicon wafer (1 g/cm of wafer diameter). The PDMS was left for about a minute to allow it to spread over the whole area of the wafer; the wafer may be rocked or spin-coated to facilitate the spreading of the PDMS prepolymer. A silane-treated PDMS blanket (8−10 mm thick) was carefully placed on top of the PDMS prepolymer. To avoid air bubbles from being trapped between the PDMS prepolymer and PDMS blanket, we aligned the edge of the PDMS blanket to the edge of the silicon wafer and slowly rolled it over the wafer to the other edge. The assembly of the PDMS blanket and prepolymer on the silicon wafer was transferred to a vacuum chamber. A weight of about 8 lbs was placed on top of the PDMS blanket and the assembly was subject to vacuum for up to 5 min. The weight was carefully placed to avoid damaging SU8 features. After vacuuming, the weight may be reduced to about 3 lbs., after which the assembly was incubated at 72 °C for 2 h to cure the PDMS prepolymer sandwiched between the wafer and PDMS blanket. To fabricate the divider box, we explored 3D printing, computer numerical control (CNC) machining, and fabrication using PDMS. To fabricate a PDMS-based divider box, a PMMA mold for the divider box was fabricated using CNC machining, cleaned in isopropyl alcohol, and dried using nitrogen gas. PDMS prepolymer was cast over the PMMA mold and cured at 72 °C for 2 h. After curing, the PDMS was stripped from the mold. The space between through-pores on the PDMS substrate was patterned with glass microspheres/beads (1.9 μm diameter), either by depositing directly onto the PDMS substrate or depositing them on poly-D-lysine-coated coverslips. The divider box was then bonded to the PDMS substrate with through-pores and the glass coverslip by plasma bonding.

2.2. Characterization of Fluidic Isolation between Device Compartments. To characterize possible diffusion of growth factors (used in cell culture) between compartments in the device, we compared diffusion of dye between compartments in devices with divider boxes made by 3D printing, PMMA, and PDMS. Devices were rinsed with deionized (DI) water, and two diagonal compartments in the device were filled with Rhodamine B (Sigma-Aldrich, 83689) in DI water (0.1 mM). The other two diagonal compartments were filled with DI water. The devices were incubated at 37 °C for 36 h. Two hundred microliters of water was drawn from the water compartments in each device (100 μL per compartment) and added to fresh DI water to 1 mL volume in standard methylacrylate cuvettes (Fisher Scientific; Pittsburgh, PA). Fluorescence measurements were performed using a fluorospectrometer (model RF-1501, Shimadzu; Kyoto, Japan). As controls we also measured fluorescence of freshly mixed dye and for dye and DI water, which were separately incubated in the devices for 36 h.

2.3. Preparation of Devices for Cell Culture. The devices were prepared for cell culture by rinsing with phosphate-buffered solution once, followed by incubation with cell culture medium at 37 °C overnight and phosphate-buffered solution for 4−8 h. The devices were then incubated at 37 °C with 15 μg/mL of laminin (Invitrogen, 23017-015) in phosphate-buffered solution overnight and rinsed twice with growth medium before seeding with cells.

2.4. Stem Cell Culture and Differentiation. We used human-induced pluripotent neural stem cells (hipNSCs) purchased from MTI-Global stem (GSC-4301). The cells were maintained in Neurobasal medium (Life Technologies 21103-049), 0.1% non-essential amino acids (corning Cellgro 25-025-Cl), 2 mM L-alanine/L-glutamine (Glutamax, Corning Cellgro 25-015-Cl), and B-27 supplement (Life Technologies 17504-044). In hipNSC cultures intended to be directed toward GABAergic phenotype, we supplemented the base medium with bFGF2. We adapted Perrier et al. protocol for derivation of midbrain dopaminergic neurons.[20] Briefly, stem cells were maintained in the base medium and supplemented with sonic hedgehog (SHH), fibroblast growth factor-8a (FGF8), brain-derived neurotrophic factor (BDNF), and ascorbic acid (AA). Neural stem cells were maintained with medium changes every 2 days, and differentiation was initiated at passage 5. We initiated differentiation of GABAergic neurons by maintaining cells in base medium in the absence of bFGF2, while differentiation in dopamine-intended neurons was initiated by the withdrawal of both FGF8 and SHH from the dopamine medium. The differentiation medium consisted of base medium supplemented with BDNF, AA, glial cell line-derived neurotrophic factor (GDNF), dibutyl cAMP, and transforming growth factor type β3 (TGF-β3). Medium changes were performed every 3 days.

2.5. Immunohistochemistry. Cultures were fixed in 4% paraformaldehyde (wt/vol) in phosphate-buffered solution followed by permeabilization with ice-cold methanol. The samples were blocked in 5% normal goat serum and 0.3% Triton X-100 diluted in PBS for 1 h at room temperature and incubated overnight at 4 °C with primary antibodies. The samples were washed in PBS and incubated at room temperature with secondary antibodies for 2 h before imaging. Both primary and secondary antibodies were diluted with 1% BSA and 0.3% Triton X-100 in PBS. The primary antibodies used were GFAP (rabbit, Biolegend: 840001; 1:1000), Tuj1 (chicken, Abcam: ab107216; 1:500), nestin (mouse, Biolegend: 656802; 1:200), GABA (mouse, Sigma: A0310; 1:2000), tyrosine hydroxylase (sheep, Life Technologies: PA14679; 1:2000), and vGlut1 (rabbit, Life Technologies: 482400; 1:2000). The cell nuclei were stained with DAPI (300 nM, life Technologies: D1206). We used Alexa 488 (Abcam), Alexa 594 (Abcam), Alexa 555 (Life Technologies), and Alexa 647 (Life Technologies) as secondary antibodies.

2.6. Calcium Imaging. A 5 μM flou-4 solution (Life Technologies, F14201) containing 0.01% pluronic F-127 (Life Technologies, P3000MP) and 1% probenecid (Life Technologies, P36400) in 2 mL of HBSS was incubated in the device for 1 h at 37

https://dx.doi.org/10.1021/acsbiomaterials.0c00895
ACS Biomater. Sci. Eng. 2021, 7, 350−359

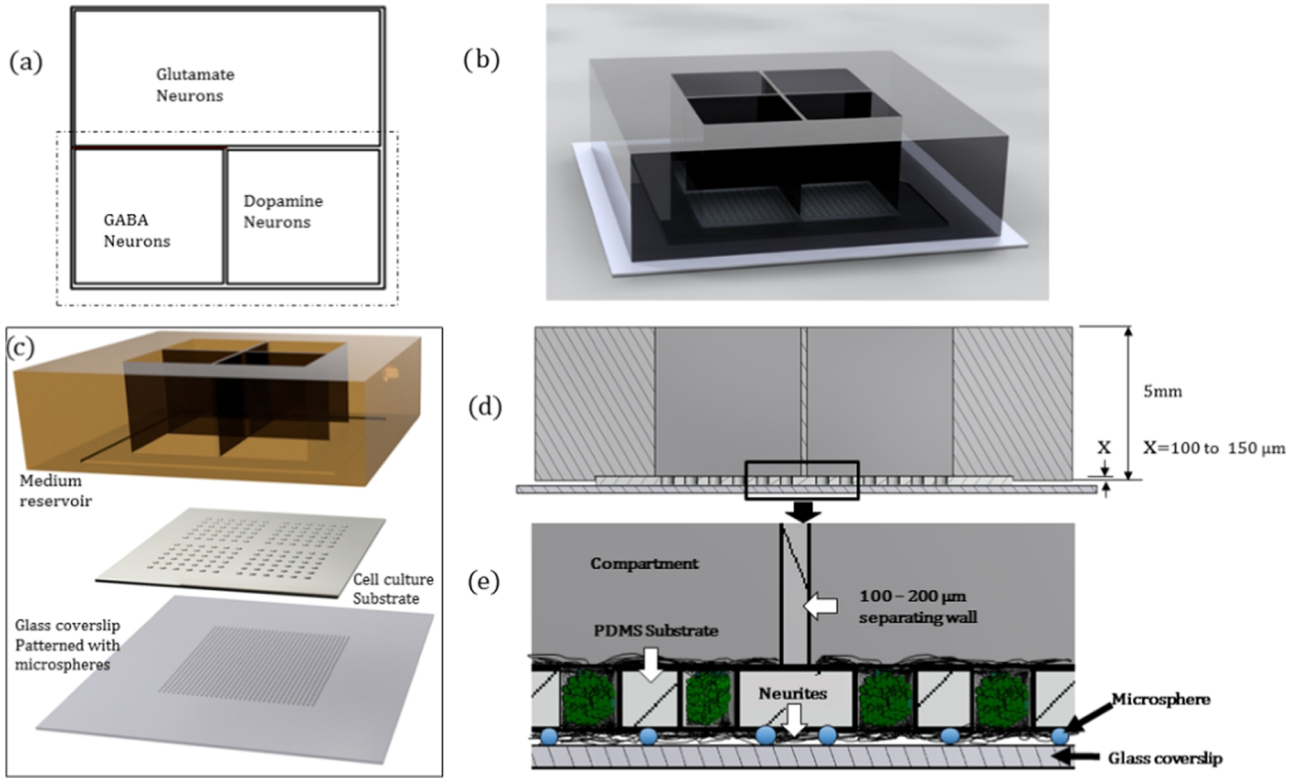

Figure 1. Device Design. (a) Schematic of a device design concept for modeling functional neuronal connectivity based on Carlson et al.'s brake and accelerator theoretical framework for schizophrenia. The partition emphasizes the focus for the proof of concept presented in this study. (b) Translation of the design concept into a scalable microdevice model. (c) Exploded-view illustration of the components of the microdevice: a compartmentalized medium reservoir, cell culture substrate with an array of through-channels or holes for containing neurospheres, microspheres that are spacers for neurites to grow through, and glass coverslip. (d, e) Section views of the device to demonstrate key dimensions for the device and possible network morphology in the device. d) shows the intersection of the three components in (c), which is magnified further in (e) green represents neurospheres in the channel or holes. Maturation of neurons to different phenotypes is facilitated by a compartmentalized culture design, while neurospheres can freely extend neurites to neighboring neurospheres via spaces created by microspheres trapped under the cell culture substrate.

°C. The cells were washed in HBSS and then incubated in HBSS with 1% probenecid for 45 min at room temperature. Cellular calcium data was acquired by laser scanning microscopy through a 20× objective of an inverted microscope (Nikon Eclipse TE300) through a 505 nm long pass filter of a 488 nm confocal laser scanning unit. The images were acquired using SimplePCI software at a rate of 1.37−2 frames per second.

3. RESULTS AND DISCUSSION

3.1. Device Design and Description. The device design is inspired by Carlsson et al. "brake and accelerator model for schizophrenia", which presents dopamine transmission (from VTA) as the central "vehicle" for the disease and glutamate (PFC) and GABA transmission (striatum/NAc) as the accelerator and brake, respectively.[21] We translated this model to a construct in which functionally connected regions may be idealized as anatomically connected. Figure 1a shows a schematic of a microdevice concept design with compartments in which different neuronal phenotypes may be derived simultaneously and allowed to connect to mimic multiple neurotransmission projections (such as PFC, VTA, and NAc regions in the Carlsson et al. model). As a proof of concept, we attempted to model circuits between the VTA and the NAc, whose major cell populations are dopamine neurons and GABA neurons, respectively.

A key challenge with industrialization of lab/organ-on-a-chip microsystems is the robustness of setups often involving micromechanical valves and perfusion systems.[22,23] Such complexity may impose minimum skill requirement as well as limit the miniaturization of such microsystems and their adoption in combinatorial cell-based assays in drug discovery. In this design, we developed a perfusion-free microsystem to make the device amenable to scale-up and integration with multiwell plate dishes, which we demonstrate in Figure 1b. Figure 1c,d shows the components of the device, which consist of a glass coverslip patterned with microspheres and the cell culture substrate with an array of through-holes. We utilized 100−200 μm diameter pores on 5−10 mm^2 grid to demonstrate the ability to scale the device. To facilitate derivation and maintenance of different neuronal phenotypes on the same substrate, the design compartmentalizes the cell culture area using a divider box. Different growth factors and signaling effector molecules can be applied to compartments. This results in exposure of neural stem cells in each compartment to different chemical gradients, which direct stem cells to different neuronal phenotypes. Also, as illustrated in Figure 1e, when neurons are seeded in the cell substrate pores, they aggregate to form neurospheres, which are constrained in the array of through-pores in the PDMS substrate. Microspheres on a glass coverslip prevent the PDMS membrane from bonding to glass in the area where microspheres were patterned. This creates a spacer between the PDMS substrate and glass coverslip through which

https://dx.doi.org/10.1021/acsbiomaterials.0c00895
ACS Biomater. Sci. Eng. 2021, 7, 350−359

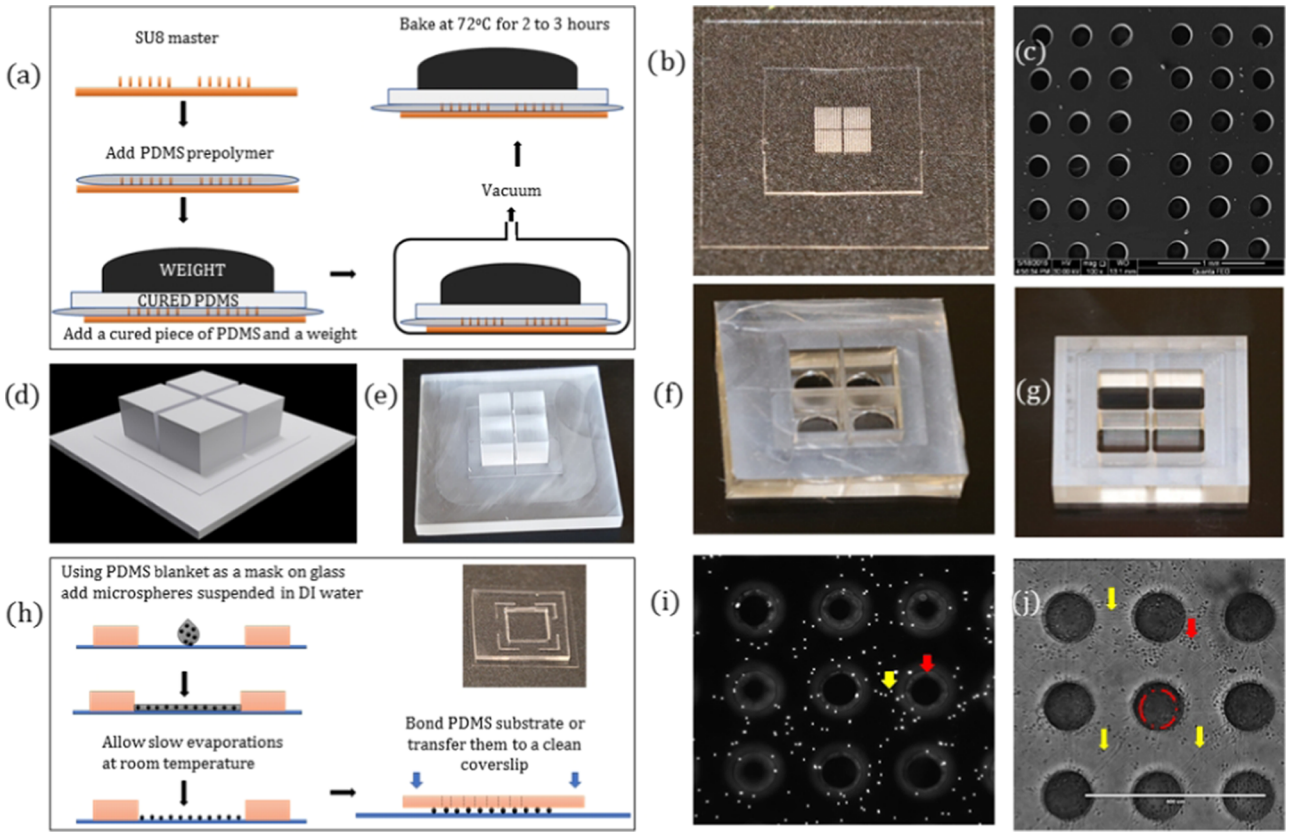

Figure 2. Device fabrication: (a) Schematic of the fabrication process for the PDMS-based cell culture substrate with through-pores. (b) Demonstration of the PDMS-based cell culture substrate bonded to glass. (c) Close-up view of an SEM micrograph of the PDMS substrate showing through-pores. (d) Illustration of a mold used to fabricate the PDMS-based divider box. (e) PDMS divider box mold as fabricated by CNC machining of PMMA. (f) Image of the PDMS divider box, (g) CNC-machined divider box (right). (h) Single-layer deposition technique used to pattern glass microspheres on glass coverslips. The inset on the top right shows a coverslip with a PDMS blanket mask shielding the area not to be patterned with microspheres. (i) Typical distribution of microspheres (yellow arrow) in relation to pores (red arrow) in the PDMS substrate. (j) demonstrates that channels/holes immobilize cell somas to facilitate formation of neurospheres (red circle), while the microspheres (red arrow) act as spacers to allow multidirectional growth of neurites (yellow arrows) between the PDMS substrate and the glass coverslip.

neurospheres extend their axonal and neurite branches in all directions to connect with neighboring neurospheres.

3.2. Fabrication and Characterization. The cell culture substrate was fabricated using PDMS. We utilized conventional soft-photolithography techniques[24,25] to fabricate an SU8 mask, which we used to create thin PDMS membranes with through-pores. Li et al. study[26] explained that Folch's et al. technique[27] leaves a thin PDMS membrane on top of the holes and demonstrated a method that assembles the mold and a PDMs sacrificial layer and deposits the PDMS prepolymer on the setup that flows into the space between them. However, our experiments showed that this technique is unreliable in fabrication of thin substrates of about 200 μm due to slow flow of PDMS between the mold and a PDMs sacrificial layer and entrapment of air bubbles in the PDMS prepolymer. We developed a simple and repeatable methodology that hybridizes Li et al. and Folch et al. techniques to achieve through-pores through substrates, which we demonstrate in Figure 2a. Briefly, our method cast the PDMS prepolymer on the mold onto which a thick silane-treated PDMS blanket was laid. A weight was added to the assembly in a vacuum chamber and vacuum was applied to the assembly for 2−5 min. After the PDMS prepolymer was left to cure, it formed a thin substrate with through-pores, as illustrated in Figure 2b,c. We fabricated substrates of varying thicknesses (182 ± 5.6, 209 ± 8.9, and 260 ± 4.9 μm) by changing the height of features on the SU8 master and vacuum time.

We fabricated the divider box using three methods: 3D printing, computer-controlled cutting (CNC machining) of poly(methyl methacrylate) (PMMA), and PDMS. The PDMS compartment box was fabricated by casting the PDMS prepolymer on a CNC-machined mold (Figure 2d,e). To facilitate the release of cured PDMS from PMMA mold, we adopted a tapered reservoir design. Figure 2f,g shows pictures of divider boxes fabricated using PDMS and PMMA, respectively. To pattern glass microspheres between through-pores of the substrate, we developed a strategy inspired by nanosphere lithography techniques.[28−32] Figure 2h demonstrates a single-layer deposition technique used to pattern glass microspheres/beads on glass coverslips. Briefly, glass microspheres (1.9 μm diameter) were treated with surfactant and suspended in DI water. A droplet of DI water containing the glass microspheres was deposited on glass and allowed to evaporate slowly. Rapid evaporation/drying caused an uneven distribution of microspheres on the coverslips (data not shown). The pattern showed in Figure 2i is a typical result of either bonding the PDMS substrate to glass patterned with glass beads and shedding excess beads by sonication or by transferring the beads to the PDMS substrate by gently pressing the substrate over glass patterned with the micro-

https://dx.doi.org/10.1021/acsbiomaterials.0c00895
ACS Biomater. Sci. Eng. 2021, 7, 350−359

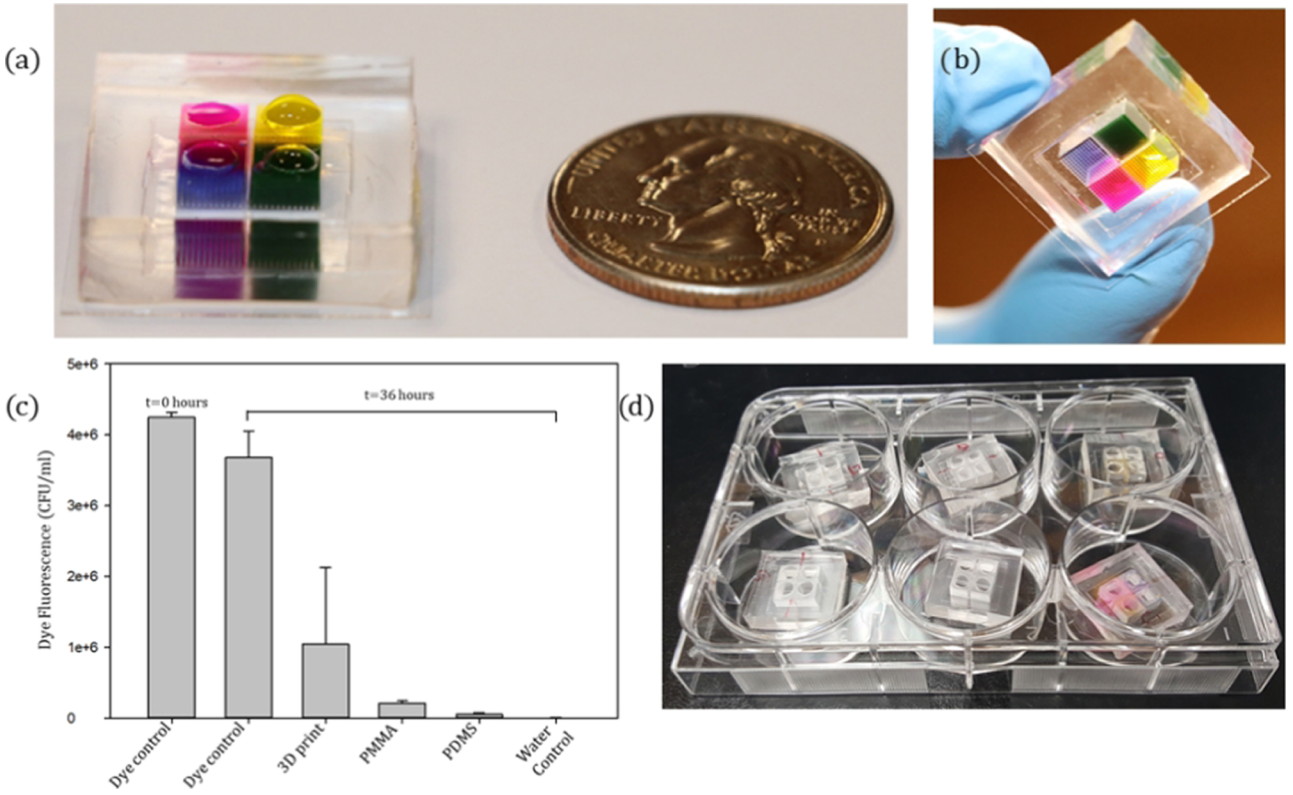

Figure 3. (a) Photograph of the device next to a USA quarter (diameter, 24.26 mm) for size comparison. The (green, blue, pink, and yellow) dyes show the different compartments. (b) Picture taken from the base of the device to show the substrate with through-pores. (c) Half of the device was filled with Rhodamine B dye and the other half incubated with water. After 36 h, we tested for diffusion of dye to the water compartments by measuring dye fluorescence in compartments of the device initially filled with water. Devices with 3D-printed compartments showed higher diffusion in comparison to devices with PMMA and PDMS compartments. The runs were replicated at least three times and the error bars are standard deviation. (d) Illustration of the setup of devices in a multiwell plate. A device with negligible diffusion is preferred as differentiating agents from one chamber are restricted to that chamber, where multiple neurotransmitter systems are being generated in the same device.

spheres before bonding it to a clean coverslip. As shown by the picture in Figure 2j, this simple technique was sufficient to create space between the substrate and the glass coverslip while allowing free extension of neurites from neurospheres constrained in the pores of the substrate.

The components were bonded by pressing parts together after exposure to oxygen plasma. Images in Figure 3a,b show the device after assembly. To facilitate bonding of PDMS cell culture substrates with 3D-printed and PMMA-based boxes, the boxes were pretreated with (3-aminopropyl) triethoxysilane (APTES), using an organo-silanization technique,[33,34] prior to plasma treatment. We tested for diffusion between compartments at atmospheric pressure by incubating half of the device with rhodamine B and the other half with water. After 36 h, we estimated the level of diffusion between compartments by measuring the change in fluorescence in water incubated in devices fabricated using 3D-printed, PMMA-, and PDMS-based divider boxes. As shown in Figure 3c, devices with PMMA- and PDMS-based divider boxes showed minimal diffusion of dye between compartments compared to devices with 3D-printed compartment boxes. Moreover, fabrication with PMMA and PDMS allowed for control of compartment wall thickness to 100 μm, which was not possible in 3D-printed devices. Due to high cost and time requirements for micromachining PMMA, coupled with extra steps involved in PMMA−PDMS bonding, we utilized PDMS-based compartment boxes in our cell culture experiments. The assembled devices were prepared for cell culture by sterilization under UV light in a biosafety cabinet for 12 h (both the top and bottom sides were directly exposed to UV light for 6 h each) or by ethylene oxide sterilization and placed in multiwell plates (as shown in Figure 3d). To eliminate air bubbles from pores in the substrate and reduce effects of PDMS's absorption of small molecules[35,36] and release of toxic leachables[37] during culture, the devices were supersaturated[38] through incubation, first with the medium for overnight at 37 °C and then with phosphate-buffered solution for 4−8 h at 37 °C, prior to coating with laminin.

3.3. Cell Culture. We cultured human neural stem cells in poly-D-lysine-laminin-coated T75 flasks and initiated terminal differentiation to dopamine neurons and GABA neurons in separate experimental setups. We adopted neuronal phenotype derivation protocols previously developed in other studies.[20,39] Briefly, GABA neurons were derived from neural stem cells previously maintained in the FGF2-supplemented medium. Terminal differentiation was initiated by a subsequent withdrawal of FGF2 from the medium. Specification toward midbrain dopamine neurons was achieved by supplementing neural stem cell medium with SHH and FGF8 and later differentiated in medium containing BDNF, GDNF, TGF-β3 ascorbic acid, and cyclic-AMP. On day 12 of differentiation, the cells were passaged and seeded into the device at a density of 2.5×10^5 per compartment; each phenotype was seeded in two adjacent compartments of the device. We experimented with initiating differentiation of stem cells in the device, rather than seed neurons after 12 days of differentiation, but the rapid

https://dx.doi.org/10.1021/acsbiomaterials.0c00895
ACS Biomater. Sci. Eng. 2021, 7, 350−359

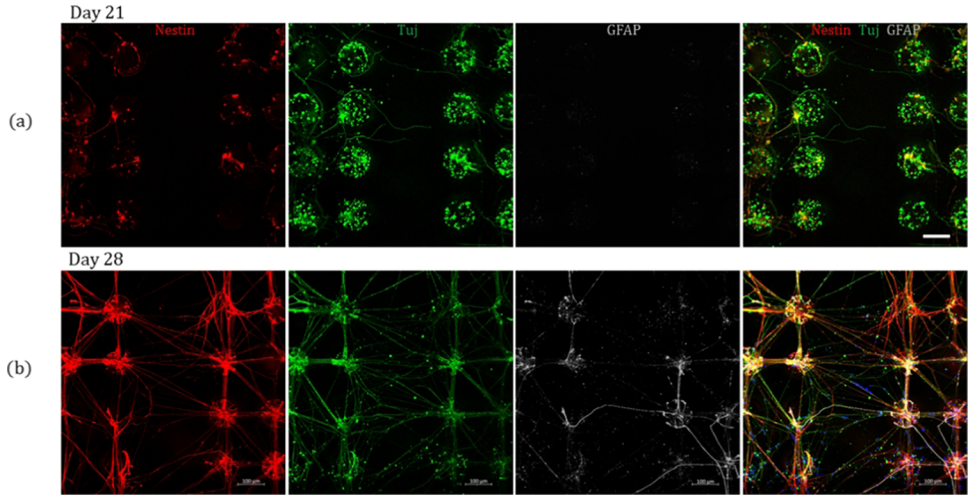

Figure 4. Specification of neuronal fate in the device. Passage 5 neural stem cells were separately directed toward dopaminergic and GABAergic differentiation. Twelve days after neural induction, the cells were seeded in the microdevice. (a) At 21 days, immunochemistry for Nestin (red), Tuj1 (green), and GFAP (gray) revealed that less than 50% (n = 38) of the neurospheres had extended neurites to neighboring compartments. (b) On day 28, a significant increase in the astrocyte population and about 92.5% connectivity between neurospheres across compartments (n = 40) was shown. Scale bars are 100 μm.

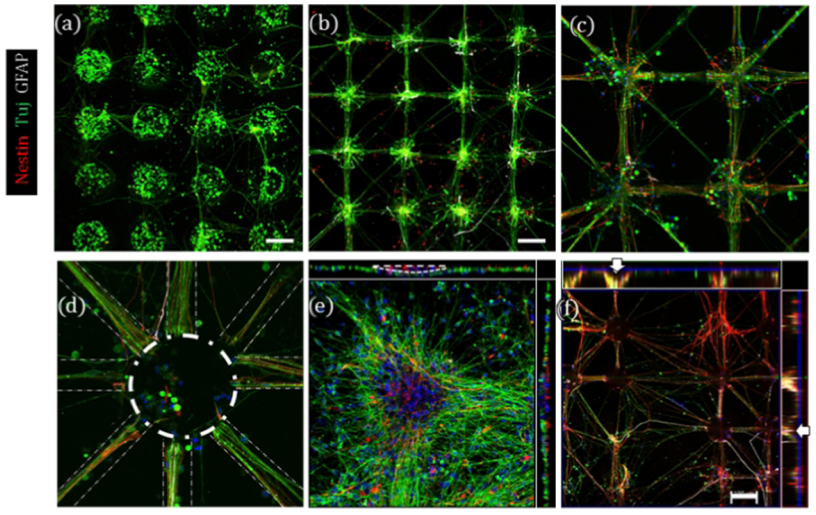

Figure 5. Neurosphere network structure and microtissue morphology. (a) Neurospheres extended neurites in random directions to form unrestricted connections early in culture (as shown in the image after 21 days of differentiation). (b) After prolonged culture, the neurospheres aggregated more with bundled fibers to connect to almost all of the closest neighbors in star-like patterns. (c) Magnified view of cultures at 45 days shows casing axonal bundling. (d) Neurospheres rearranged and bundled their fibers as though they are constrained in channels, the dotted lines emphasize rearrangement of axonal bundles to form a star-like pattern and appear as though restricted in channels. (e, f) Microtissues in both freely cultured neurospheres (e) and those cultured in our substrate (f), rearranged cells such that Tuj$^+$ cells were at the periphery of the spheroids, while Nestin$^+$ cells (highlighted with image sections in boxes on top and right in (e)) were located at the core. In the sections, top of the section is the glass/substrate surface. Nestin (red) is more in the center and Tuj (green) is more on the outskirts. Also, as shown by arrows in (f), the neurospheres were increasingly observed to detach from the substrate starting at 42 days after differentiation. Cell nuclease is indicated by DAPI staining in d and f. Scale bars are 50 μm.

proliferative behavior of neural stem cells at the beginning of differentiation made control of cell number (and microtissue size) difficult and led to rapid exhaustion of medium as well. After induction of differentiation, the proliferation of neural stem cells is gradually reduced as active notch signaling is deactivated. Inhibition of notch signaling increases the neurogenic potential of stem cells, which causes cells to embark on differentiation to a neuronal lineage, a process that has been reported to slow down significantly at 16 days in vitro, after which glial differentiation is induced.[40]

Aggregation of cells in the pores of the substrate was induced by application of slight centrifugation (at 10g, for 1−5 min), and medium changed every 3 days. We assessed the composition of cultures 21 days after neural induction using antiglial fibrillary acidic protein (GFAP), β-tubulin, class III (Tuj) and Nestin, which stain for astrocytes, neurons, and neural stem cells, respectively. We observed that less than 50% Tuj$^+$ neurospheres extended neurites across compartments (n = 38 random neurospheres from 4 devices), but almost all of the neurospheres extended nerve fibers to at least one neighboring neurosphere in the same compartment. By day

https://dx.doi.org/10.1021/acsbiomaterials.0c00895
ACS Biomater. Sci. Eng. 2021, 7, 350−359

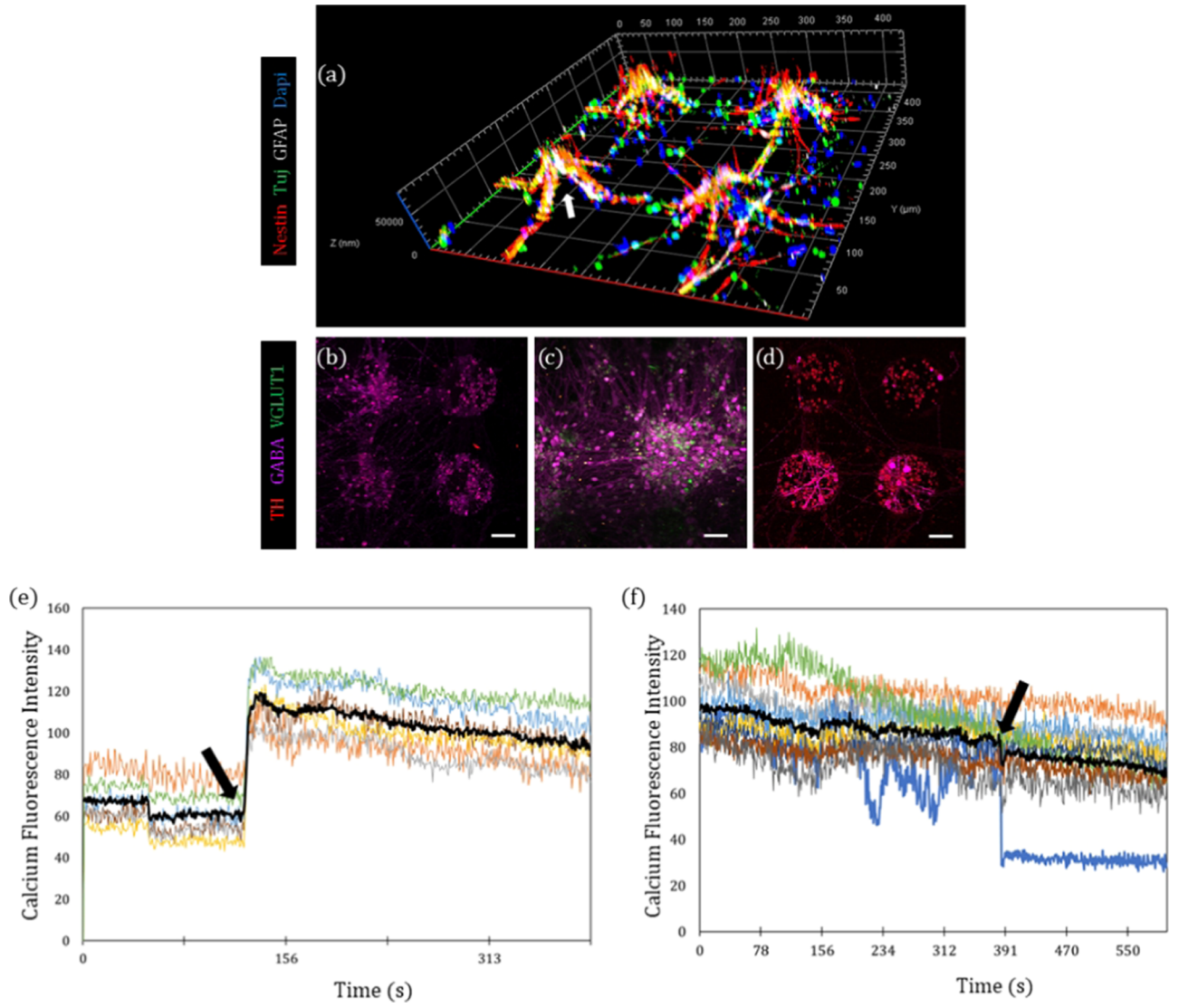

Figure 6. Phenotypic characterization of neurons: (a) 3D image to illustrate the tendency of the neurospheres to detach from the coverslip and migrate upward into the pores at later days of culture. (b) TH, GABA, and Vglut1 expression in the GABAergic compartment 42 days after induction of differentiation. (c) Vglut1$^+$ cells were observed at the top of some spheroids in the GABAergic compartment on day 45. (d) TH, GABA, and Vglut1 expression in the dopamine compartment 42 days after induction of differentiation. Scale bars are 100 μm. (e) Depolarization of dopaminergic neurons using a high K^+ buffer resulted in a rapid increase in mean intracellular calcium fluorescence magnitude in compartments with GABAergic neurons. (f) Depolarization of GABAergic neurons using a high K^+ buffer resulted in a rapid depression of mean intracellular calcium fluorescence in dopaminergic neurons. The mean intracellular calcium fluorescence magnitude is shown by black traces in (e) and (f) – n = 6 cells and n = 9 cells, respectively. A black arrow indicates the point at which a high K^+ buffer was injected.

28, almost all neurospheres at the borders of the compartments extended a high density of fibers to connect with neurospheres across the compartment, as shown in Figure 4a,b for comparison. The lack of connections from some of the neurospheres was due to the bonding of PDMS to glass, which constrained neuronal fibers in the pores. Interestingly, some nestin$^+$ cells also extended neurites across compartments (Figure 4b). Also, as shown in Figure 4a, GFAP$^+$ astrocytes were a very small percentage (less than 1%) on day 21, but the number of GFAP$^+$ cells increased after prolonged differentiation in vitro (Figure 4b). This is because neural stem cells predominantly express neurogenic potential during the early days of differentiation before they switch to become glia-producing progenitors later in culture.[40] As such, the late maturation of GFAP$^+$, several weeks after differentiation has been initiated, as observed on day 28, is not unprecedented in experiments using 3D tissues. Several studies using human-derived stem cells have shown the presence of neural progenitor cells, which expressed mitotic markers and/or continued to proliferate for several weeks or months after evidence of differentiation, to neurons, was noted. For example, in Pasca et al.'s study,[8] human cortical spheroids derived from human-induced pluripotent stem cells in a suspension culture showed the presence of both actively proliferative neural progenitors and mature neuronal cells at 52 days in culture. Also, in Yan et al.'s study,[42] when human fetal spinal cord-derived neural stem cells were grafted in adult nude rats, immunoreactivity for neuronal lineage in the grafts was expressed as early as 3 weeks post grafting and GFAP reactivity was observed no earlier than 3–6 months post grafting. However, while expression of Nestin is said to have declined

https://dx.doi.org/10.1021/acsbiomaterials.0c00895
ACS Biomater. Sci. Eng. 2021, 7, 350–359

over time, this study reported that 11−14% of the grafted cells remained Nestin positive at 6 months post grafting.

3.4. Neurospheres Bundle Fibers and undergo Microtissue Arrangement Late in Culture. Li et al.[26] speculated that platforms that allow unconstrained growth of axons may result in highly physiological relevant neural networks compared to devices that provide channels to direct axonal growth. In our study, we suspended our cell culture substrate on 2 μm microspheres to provide spaces for unrestricted growth of neurites. Consistent with Li et al.'s work, neurospheres (constrained in through-pores) extended neurites in seemingly random directions and maintained this connectivity pattern through day 21 in all our devices (Figure 5a). However, as shown in Figure 5b the nature of connections between neurospheres changed dramatically between day 21 and day 30. By day 30, in 13/18 devices, the neurospheres had rearranged their processes. As illustrated in Figure 5c, we observed that projections from neurospheres seemed to bundle axons together and reach to all of their nearest neighbors in straight lines as though seeking for the shortest path in star-shaped patterns, almost as if they were constrained in channels (Figure 5d). The alignment of neuronal processes and axonal bundling to form a "starburst appearance" in freely cultured neurospheres, after prolonged differentiation in vitro has been previously reported,[41] can be seen in other literature.[9,43,44] This behavior leads us to speculate that axonal bundling may be characteristic of neuronal maturation in in vitro cultures. Consequently, contrary to Li et al.'s work, we submit that substrates with channels for axonal guidance may not affect the physiological relevance of cultures and that star-shaped channel patterns may provide sufficient connectivity for neurospheroid patterning in vitro. To rule out the distance between neurospheres as a confounding factor in the preference for connectivity, we used a pore array spacing comparable to Li et al.'s study (100 μm), but this did not alter the pattern of the neural circuits. Taken together, we suspect that the formation of random arborizations may be important for initial microenvironment sensing, but a rearrangement and bundling of networks, as though in channels, may be necessary for reinforcing neuronal circuit connections during later days in culture. On day 42, the microtissues also showed a laminar arrangement of cells with Tuj$^+$ cells at the periphery of the neurospheres, while cells in the core of the spheroids stained positive for a neuronal precursor, Nestin (Figure 5e). Moreover, most of the spheroids seemed to form hanging neurospheres embedded in through-pores in the PDMS substrate and anchored to their neighbors through their processes (Figures 5f and 6a). Such microtissue arrangements and heterogeneity in cell maturity may require the development of specialized in vitro electrophysiological recording strategies to identify and target select cell populations in microtissues.

3.5. Neuronal Phenotype Derivation in the Device (Simulation of Brain Regions in the Device). Forty two days after differentiation was induced, we checked the cultures in the device to see if they created distinct regions of dopaminergic neurons and GABAergic neurons in their respective compartments. We used antibodies for vesicular glutamate transport 1 (vGLUT1), GABA, and tyrosine hydroxylase (TH), which are subtype markers for glutamate, GABA, and dopamine neurons, respectively. As anticipated, neurons maintained in compartments with basic medium, in the absence of FGF2, mostly stained positive for GABA and vGLUT1. As can be seen in Figure 6b, only a few cells (less than 1%) stained TH$^+$. Interestingly, while neurons at the bottom of the pores were only GABA$^+$, the cells at the top of the spheroids expressed a small population of vGLUT1$^+$ cells, which we show in Figure 6c. The dominance of GABAergic neurons in this compartment makes this region a relevant in vitro model for the NAc. On the other hand, in compartments treated with BDNF, GDNF, TGF, and AA, over 50% of the cells were TH$^+$ (based on a qualitative assessment), while the rest stained positive for GABA, Figure 6d. The expression of a small percentage of GABA neurons is typical of in vitro protocols for derivation of TH$^+$ neurons. Low to medium (29−about 70%) conversion rates of neural stem cells to TH$^+$ neurons have been reported using similar protocols.[20,45,46] Also, despite the expression of GABA$^+$ neurons in compartments treated for derivation of TH$^+$ neurons, we consider the result as a relevant model for the VTA. While the projections from the VTA are often assumed to be predominantly dopaminergic, only about 55% of the neurons in this region are dopaminergic,[47,48] the composition of local neuronal population in this region consists of a substantial population of GABA neurons in vivo.[49] To check if the neurons in the different compartments made functional synapses, we stimulated neurons in the compartments using a high K$^+$ buffer (50−70 mM). We hypothesized that depolarization of microtissues in one compartment would result in millisecond timescale propagation of an action potential to different compartments and subsequent calcium response. Forty eight days after differentiation, depolarization of neurons in the dopaminergic compartment using a high K$^+$ buffer resulted in a rapid increase in mean intracellular calcium fluorescence magnitude in compartments with GABAergic neurons (Figure 6e). Interestingly, depolarization of neurons GABAergic resulted in a rapid decrease in mean intracellular calcium fluorescence in dopaminergic neurons (Figure 6f). Nicholas et al.'s study[50] reported that human pluripotent stem cell-derived 3D neuronal tissue was still electrophysiologically immature at 8 weeks. While the application of GABA has been reported to increase intracellular calcium in some studies,[51,52] electrophysiological behavior of immature neurons to GABA application (more so, via a $GABA_A$ receptor-dependent mechanism) is unpredictable;[53] it can have either depolarizing, hyperpolarizing, or negligible effect on membrane potential depending on the reversal potential of $GABA_A$ receptors in relation to the membrane potential of the cell at the time the receptor is gated by GABA. We speculate that the mean reduction in intracellular calcium may be related to hyperpolarization of cells, while individual cells that showed no calcium response had no change in membrane potential. Therefore, mixed calcium responses observed after depolarization of GABA neurons may suggest $GABA_A$ receptor-dependent calcium response. On the other hand, application of dopamine on GABAergic interneurons has been shown to facilitate calcium increases mediated by D1 dopamine receptors via inositol 1,4,5-triphsosphate (IP_3) signaling[54] or enhancement of Ca_V1 channel calcium currents,[55] which increase the excitability of the interneurons. While further experimentation is required to understand the mechanism(s) underlying calcium responses in this microsystem, the change of calcium response magnitude in compartments due to stimulation of neuronal networks in neighboring compartments in this study was sufficient to suggest that, indeed, the

https://dx.doi.org/10.1021/acsbiomaterials.0c00895
ACS Biomater. Sci. Eng. 2021, 7, 350−359

neurospheres in different compartments made functional connections.

4. CONCLUSIONS

In this study, we demonstrated a multicompartment microdevice for patterning neurospheres and specification of neural stem cell fate toward networks of two neuronal phenotypes. A multicompartment design presented allows for the application of different morphogens and growth factors to cultures to induce diverse neuronal fate. We demonstrated the capabilities of our design by formation of unrestricted robust neuronal circuits between (and across) arrays of neurospheres in all compartments of our device. Also, we speculated that our design is capable of specification of neuronal phenotypes in different compartments simultaneously, which we demonstrate by directing neuronal maturation of human neural stem cells to dopaminergic and GABAergic neurons in different compartments of the device. Dopamine−GABA projections play important roles in cognition and behavior and aberrations in dopamine−GABA transmission play a key role in diseases like schizophrenia. Schizophrenia is a typical example illness involving intricate neuronal circuits, which also characterize most neurological disorders. Therefore, such multiphenotype models may be of relevance in modeling functional interregional brain networks associated with aberrations that result from disease deficits and/or modeling neural circuitry associated with treatment side effects in vitro. From a design view, the simplicity of the design lends it to compatibility with multiwell plate systems for high density bioassays. At a microlevel, immobilization of neurospheres lends the setup to high-throughput readout, such as the multielectrode array electrophysiology, and optical readout, such as calcium imaging. Future work will develop strategies for high-throughput electrophysiological probing with considerations for microtissue cellular arrangement observed later in culture.

AUTHOR INFORMATION

Corresponding Author

William S. Kisaalita − *School of Chemical, Materials and Biomedical Engineering, University of Georgia, Athens, Athens, Georgia 30602, United States;* orcid.org/0000-0001-6999-8276; Phone: +1 706-542-0835; Email: williamk@uga.edu

Authors

Kenneth Ndyabawe − *School of Chemical, Materials and Biomedical Engineering, University of Georgia, Athens, Athens, Georgia 30602, United States*

Michael Cipriano − *Department of Biochemistry and Molecular Biology, and, University of Georgia, Athens, Athens, Georgia 30602, United States*

Wujun Zhao − *Department of Chemistry, University of Georgia, Athens, Athens, Georgia 30602, United States*

Mark Haidekker − *School of Electrical and Computer Engineering, College of Engineering, Driftmier Engineering Center, University of Georgia, Athens, Athens, Georgia 30602, United States*

Kun Yao − *School of Electrical and Computer Engineering, College of Engineering, Driftmier Engineering Center, University of Georgia, Athens, Athens, Georgia 30602, United States*

Leidong Mao − *School of Electrical and Computer Engineering, College of Engineering, Driftmier Engineering Center, University of Georgia, Athens, Athens, Georgia 30602, United States*

Complete contact information is available at: https://pubs.acs.org/10.1021/acsbiomaterials.0c00895

Notes

The authors declare no competing financial interest.

REFERENCES

(1) Brisch, R.; et al. The Role of Dopamine in Schizophrenia from a Neurobiological and Evolutionary Perspective: Old Fashioned, but Still in Vogue. *Front. Psychiatry* **2014**, *5*, 47.

(2) Olijslagers, J. E.; et al. Modulation of Midbrain Dopamine Neurotransmission by Serotonin, a Versatile Interaction Between Neurotransmitters and Significance for Antipsychotic Drug Action. *Current Neuropharmacol.* **2006**, *4*, 59−68.

(3) Zhou, L.; et al. Organization of Functional Long-Range Circuits Controlling the Activity of Serotonergic Neurons in the Dorsal Raphe Nucleus. *Cell Rep.* **2017**, *18*, 3018−3032.

(4) Mak, I. W. Y.; Evaniew, N.; Ghert, M. Lost in translation: animal models and clinical trials in cancer treatment. *Am. J. Transl. Res.* **2014**, *6*, 114−118.

(5) Seok, J.; et al. Genomic responses in mouse models poorly mimic human inflammatory diseases. *Proc. Natl. Acad. Sci. USA* **2013**, *110*, 3507−3512.

(6) Hackam, D. G.; Redelmeier, D. A. Translation of research evidence from animals to humans. *Jama* **2006**, *296*, 1727−1732.

(7) Food, U.S., *Innovation or Stagnation: Challenge and Opportunity on the Critical Path to New Medical Products*, 2004.

(8) Paşca, A. M.; et al. Functional cortical neurons and astrocytes from human pluripotent stem cells in 3D culture. *Nat. Methods* **2015**, *12*, 671−678.

(9) Shi, Y.; et al. Human cerebral cortex development from pluripotent stem cells to functional excitatory synapses. *Nat. Neurosci.* **2012**, *15*, 477−86.

(10) Vazin, T.; et al. Efficient derivation of cortical glutamatergic neurons from human pluripotent stem cells: a model system to study neurotoxicity in Alzheimer's disease. *Neurobiol. Dis.* **2014**, *62*, 62−72.

(11) Dauth, S.; et al. Neurons derived from different brain regions are inherently different in vitro: a novel multiregional brain-on-a-chip. *J. Neurophysiol.* **2017**, *117*, 1320−1341.

(12) Ndyabawe, K.; Kisaalita, W. S. Engineering microsystems to recapitulate brain physiology on a chip. *Drug Discovery Today* **2019**, *24*, 1725.

(13) Dichter, G. S.; Damiano, C. A.; Allen, J. A. Reward circuitry dysfunction in psychiatric and neurodevelopmental disorders and genetic syndromes: animal models and clinical findings. *J. Neurodev. Disord.* **2012**, *4*, 19.

(14) Ito, R.; Hayen, A. Opposing Roles of Nucleus Accumbens Core and Shell Dopamine in the Modulation of Limbic Information Processing. *J. Neurosci.* **2011**, *31*, 6001.

(15) Ikemoto, S. Brain reward circuitry beyond the mesolimbic dopamine system: A neurobiological theory. *Neurosci. Biobehav. Rev.* **2010**, *35*, 129−150.

(16) Kellendonk, C.; et al. Transient and selective overexpression of dopamine D2 receptors in the striatum causes persistent abnormalities in prefrontal cortex functioning. *Neuron* **2006**, *49*, 603−15.

(17) Mikell, C. B.; et al. The Hippocampus and Nucleus Accumbens as Potential Therapeutic Targets for Neurosurgical Intervention in Schizophrenia. *Appl. Neurophysiol.* **2009**, *87*, 256−265.

(18) Rolland, B.; et al. Resting-state functional connectivity of the nucleus accumbens in auditory and visual hallucinations in schizophrenia. *Schizophr. Bull.* **2015**, *41*, 291−9.

(19) Seeman, P. All roads to schizophrenia lead to dopamine supersensitivity and elevated dopamine D2(high) receptors. *CNS Neurosci. Ther.* **2011**, *17*, 118−32.

(20) Perrier, A. L.; et al. Derivation of midbrain dopamine neurons from human embryonic stem cells. *Proc. Natl. Acad. Sci. USA* **2004**, *101*, 12543−8.
(21) Carlsson, A.; et al. Neurotransmitter aberrations in schizophrenia: new perspectives and therapeutic implications. *Life Sci.* **1997**, *61*, 75−94.
(22) Chandrasekaran, A.; Abduljawad, M.; Moraes, C. Have microfluidics delivered for drug discovery? *Expert Opin. Drug Discovery* **2016**, *11*, 745−8.
(23) Vladisavljević, G. T.; et al. Industrial lab-on-a-chip: Design, applications and scale-up for drug discovery and delivery. *Adv. Drug Delivery Rev.* **2013**, *65*, 1626−1663.
(24) Whitesides, G. M.; et al. Soft lithography in biology and biochemistry. *Annu. Rev. Biomed. Eng.* **2001**, *3*, 335−73.
(25) Qin, D.; Xia, Y.; Whitesides, G. M. Soft lithography for micro- and nanoscale patterning. *Nat. Protoc.* **2010**, *5*, 491−502.
(26) Li, W.; et al. NeuroArray: A Universal Interface for Patterning and Interrogating Neural Circuitry with Single Cell Resolution. *Sci. Rep.* **2014**, *4*, No. 4784.
(27) Folch, A.; et al. Microfabricated elastomeric stencils for micropatterning cell cultures. *J. Biomed. Mater. Res.* **2000**, *52*, 346−53.
(28) Oh, J. R.; et al. Fabrication of wafer-scale polystyrene photonic crystal multilayers via the layer-by-layer scooping transfer technique. *J. Mater. Chem.* **2011**, *21*, 14167−14172.
(29) Hulteen, J. C.; Van Duyne, R. P. Nanosphere lithography: A materials general fabrication process for periodic particle array surfaces. *J. Vac. Sci. Technol., A* **1995**, *13*, 1553−1558.
(30) Zhang, G.; Wang, D. Colloidal Lithography—The Art of Nanochemical Patterning. *Chem. − Asian J.* **2009**, *4*, 236−245.
(31) Sivagnanam, V.; et al. Micropatterning of protein-functionalized magnetic beads on glass using electrostatic self-assembly. *Sens. Actuators, B* **2008**, *132*, 361−367.
(32) Pregibon, D. C.; Toner, M.; Doyle, P. S. Magnetically and biologically active bead-patterned hydrogels. *Langmuir* **2006**, *22*, 5122−8.
(33) Ren, Y.; et al. A Simple and Reliable PDMS and SU-8 Irreversible Bonding Method and Its Application on a Microfluidic-MEA Device for Neuroscience Research. *Micromachines* **2015**, *6*, 1923.
(34) Lee, K. S.; Ram, R. J. Plastic-PDMS bonding for high pressure hydrolytically stable active microfluidics. *Lab Chip* **2009**, *9*, 1618−24.
(35) van Meer, B. J.; et al. Small molecule absorption by PDMS in the context of drug response bioassays. *Biochem. Biophys. Res. Commun.* **2017**, *482*, 323−328.
(36) Chumbimuni-Torres, K. Y.; et al. Adsorption of Proteins to Thin-Films of PDMS and Its Effect on the Adhesion of Human Endothelial Cells. *RSC Adv.* **2011**, *1*, 706−714.
(37) Regehr, K. J.; et al. Biological implications of polydimethylsiloxane-based microfluidic cell culture. *Lab Chip* **2009**, *9*, 2132−2139.
(38) Randall, G. C.; Doyle, P. S. Permeation-driven flow in poly(dimethylsiloxane) microfluidic devices. *Proc. Natl. Acad. Sci. USA* **2005**, *102*, 10813−10818.
(39) Hartfield, E. M.; et al. Physiological Characterisation of Human iPS-Derived Dopaminergic Neurons. *PLoS One* **2014**, *9*, No. e87388.
(40) Abranches, E.; et al. Neural Differentiation of Embryonic Stem Cells In Vitro: A Road Map to Neurogenesis in the Embryo. *PLoS One* **2009**, *4*, No. e6286.
(41) Zhang, S. C.; et al. In vitro differentiation of transplantable neural precursors from human embryonic stem cells. *Nat. Biotechnol.* **2001**, *19*, 1129−33.
(42) Yan, J.; et al. Extensive neuronal differentiation of human neural stem cell grafts in adult rat spinal cord. *PLoS Med.* **2007**, *4*, No. e39.
(43) Niclis, J. et al. Characterization of forebrain neurons derived from late-onset Huntington's disease human embryonic stem cell lines *Front. Cell. Neurosci.* 2013, 737 DOI: 10.3389/fncel.2013.00037.
(44) Jo, A. Y.; et al. Contrasting and brain region-specific roles of neurogenin2 and mash1 in GABAergic neuron differentiation in vitro. *Exp. Cell Res.* **2007**, *313*, 4066−4081.
(45) Yan, Y.; et al. Directed differentiation of dopaminergic neuronal subtypes from human embryonic stem cells. *Stem Cells* **2005**, *23*, 781−90.
(46) Jiang, H.; et al. Cell cycle and p53 gate the direct conversion of human fibroblasts to dopaminergic neurons. *Nat. Commun.* **2015**, *6*, No. 10100.
(47) Margolis, E. B.; et al. The ventral tegmental area revisited: is there an electrophysiological marker for dopaminergic neurons? *J. Physiol.* **2006**, *577*, 907−924.
(48) Margolis, E. B.; et al. Reliability in the Identification of Midbrain Dopamine Neurons. *PLoS One* **2010**, *5*, No. e15222.
(49) Margolis, E. B.; et al. Identification of Rat Ventral Tegmental Area GABAergic Neurons. *PLoS One* **2012**, *7*, No. e42365.
(50) Nicholas, C. R.; et al. Functional maturation of hpsc-derived forebrain interneurons requires an extended timeline and mimics human neuronal development. *Cell Stem Cell* **2013**, *12*, 573−586.
(51) Doengi, M.; et al. GABA uptake-dependent Ca(2+) signaling in developing olfactory bulb astrocytes. *Proc. Natl. Acad. Sci. USA* **2009**, *106*, 17570−17575.
(52) Haugh-Scheidt, L.; et al. GABA transport and calcium dynamics in horizontal cells from the skate retina. *J. Physiol.* **1995**, *488*, 565−576.
(53) Herbison, A. E.; Moenter, S. M. Depolarising and hyperpolarising actions of GABA(A) receptor activation on gonadotrophin-releasing hormone neurones: towards an emerging consensus. *J. Neuroendocrinol.* **2011**, *23*, 557−569.
(54) Swapna, I.; et al. Differential Dopamine Regulation of Ca(2+) Signaling and Its Timing Dependence in the Nucleus Accumbens. *Cell Rep.* **2016**, *15*, 563−573.
(55) Rendón-Ochoa, E. A.; et al. Calcium currents in striatal fast-spiking interneurons: dopaminergic modulation of Ca_V1 channels. *BMC Neurosci.* **2018**, *19*, 42.

https://dx.doi.org/10.1021/acsbiomaterials.0c00895
ACS Biomater. Sci. Eng. 2021, 7, 350−359